expand (Supplementary Information). It is important to recognize that further work is required to establish empirically how the absolute and proportional area losses of individual species (in other words, the type of data from climate envelope projections) are related to extinction risk. As yet, no agreed standard method exists for such calculations: assumptions and uncertainties inherent in the three methods will be considered in detail elsewhere.

Extinction probability estimates were not available for all scenarios in every region/taxon, so means of scenarios were calculated after using a least-squares analysis of variance model to impute missing values. Region/taxon mean probabilities of extinction for each scenario were logit-transformed and a three-way analysis of variance was fitted (region/taxon × climate scenario × dispersal scenario; weighted by $\sqrt{N_{\text{species}}}$ per region/taxon study). The fitted model was used to impute expected values of the probability of extinction for those region/taxon and scenario combinations for which direct estimates were not available. Scenario means were then calculated from the combined direct estimates and imputed values, using $\sqrt{N_{\text{species}}}$ for each region/taxon as weights.

Red Data Book criteria

Each species is assigned to a threat category[16], or classified 'Not Threatened' (0% risk), depending on the projected decline in area over 50 or 100 years (Supplementary Information) and the final distribution area. Existing areas were considered, so we present only the extra extinction attributable to climate change. Logit-transformed three-way analysis of variance was used to estimate extinction risks for empty cells, as with the species–area approaches.

Extinct: species with a projected future area of zero (100% of species assumed to be committed to eventual extinction).

Critically endangered: projected future distribution area $<10\,\text{km}^2$, or decline by $>80\%$ in 50 years (species assigned a 75% chance of extinction[16]).

Endangered: projected area 10–500 km^2, or 50–80% decline in 50 years (species assigned a 35% chance of extinction[16]).

Vulnerable: projected area 500–2,000 km^2, or $>50\%$ decline in 100 years on the basis of linear extrapolation of 50-year projection (species assigned a 15% chance of extinction[16]).

Received 10 September; accepted 13 October 2003; doi:10.1038/nature02121.

1. Parmesan, C. & Yohe, G. A globally coherent fingerprint of climate change impacts across natural systems. *Nature* **421,** 37–42 (2003).
2. Root, T. L. *et al.* Fingerprints of global warming on wild animals and plants. *Nature* **421,** 57–60 (2003).
3. Pounds, J. A., Fogden, M. L. P. & Campbell, J. H. Biological response to climate change on a tropical mountain. *Nature* **398,** 611–615 (1999).
4. Overpeck, J., Whitlock, C. & Huntley, B. in *Paleoclimate, Global Change and the Future* (eds Alverson, K., Bradley, R. & Pedersen, T.) 81–103 (Springer, Berlin, 2002).
5. Benton, M. J. & Twitchett, R. J. How to kill (almost) all life: the end-Permian extinction event. *Trends Ecol. Evol.* **18,** 358–365 (2003).
6. Houghton, J. T. *et al. Climate change 2001: the Scientific Basis. Contributions of Working Group I to the Third Assessment Report of the Intergovernmental Panel on Climate Change* (Cambridge Univ. Press, 2001).
7. Bakkenes, M., Alkemade, J. R. M., Ihle, F., Leemans, R. & Latour, J. B. Assessing effects of forecasted climate change on the diversity and distribution of European higher plants for 2050. *Global Change Biol.* **8,** 390–407 (2002).
8. Beaumont, L. J. & Hughes, L. Potential changes in the distributions of latitudinally restricted Australian butterfly species in response to climate change. *Global Change Biol.* **8,** 954–971 (2002).
9. Erasmus, B. F. N., van Jaarsveld, A. S., Chown, S. L., Kshatriya, M. & Wessels, K. Vulnerability of South African animal taxa to climate change. *Global Change Biol.* **8,** 679–693 (2002).
10. Midgley, G. F., Hannah, L., Rutherford, M. C. & Powrie, L. W. Assessing the vulnerability of species richness to anthropogenic climate change in a biodiversity hotspot. *Global Ecol. Biogeogr.* **11,** 445–451 (2002).
11. Peterson, A. T. *et al.* Future projections for Mexican faunas under global climate change scenarios. *Nature* **416,** 626–629 (2002).
12. Williams, S. E., Bolitho, E. E. & Fox, S. Climate change in Australian tropical rainforests: an impending environmental catastrophe. *Proc. R. Soc. Lond. B* **270,** 1887–1892 (2003).
13. Rosenzweig, M. L. *Species Diversity in Space and Time* (Cambridge Univ. Press, 1995).
14. Brooks, T. M., Pimm, S. L. & Oyugi, J. O. Time lag between deforestation and bird extinction in tropical forest fragments. *Conserv. Biol.* **13,** 1140–1150 (1999).
15. Brooks, T. M., Pimm, S. L. & Collar, N. J. Deforestation predicts the number of threatened birds in insular Southeast Asia. *Conserv. Biol.* **11,** 382–394 (1997).
16. *IUCN Red List Categories and Criteria*, version 3.1. (IUCN Species Survival Commission, Gland, Switzerland, 2001).
17. Gaston, K. J., Blackburn, T. M. & Goldewijk, K. K. Habitat conversion and global avian biodiversity loss. *Proc. R. Soc. Lond. B* **270,** 1293–1300 (2003).
18. Achard, F. *et al.* Determination of deforestation rates of the world's humid tropical forests. *Science* **297,** 999–1002 (2002).
19. Myers, N., Mittermeier, R. A., Mittermeier, C. G., da Fonseca, G. A. B. & Kent, J. Biodiversity hotspots for conservation priorities. *Nature* **403,** 853–858 (2000).
20. Roget, M., Richardson, D. M., Cowling, R. M., Lloyd, J. W. & Lombard, A. T. Current patterns of habitat transformation and future threats to biodiversity in terrestrial ecosystems of the Cape Floristic Region, South Africa. *Biol. Conserv.* **112,** 63–85 (2003).
21. Woodward, F. I. Potential impacts of global elevated CO_2 concentrations on plants. *Curr. Opin. Plant Biol.* **5,** 207–211 (2002).
22. Bond, W. J., Midgley, G. F. & Woodward, F. I. The importance of low atmospheric CO_2 and fire in promoting the spread of grasslands and savannas. *Global Change Biol.* **9,** 973–982 (2003).
23. Whittaker, J. B. Impacts and responses at population level of herbivorous insects to elevated CO_2. *Eur. J. Entomol.* **96,** 149–156 (1999).
24. Sala, O. E. *et al.* Biodiversity—global biodiversity scenarios for the year 2100. *Science* **287,** 1770–1774 (2000).
25. Lackner, K. S. A guide to CO_2 sequestration. *Science* **300,** 1677–1678 (2003).
26. Beerling, D. J. The impact of temperature on the northern distribution limits of the introduced species *Fallopia japonica* and *Impatiens glandulifera* in north-west Europe. *J. Biogeog.* **20,** 45–53 (1993).
27. Baker, R. H. A. *et al.* The role of climatic mapping in predicting the potential geographical distribution of non-indigenous pests under current and future climates. *Agric. Ecosyst. Environ.* **82,** 57–71 (2000).
28. Peterson, A. T. & Vieglais, D. A. Predicting species invasions using ecological niche modeling. *BioScience* **51,** 363–371 (2001).
29. Pearson, R. G. & Dawson, T. P. Predicting the impacts of climate change on the distribution of species: are bioclimate envelope models useful? *Global Ecol. Biogeog.* **12,** 361–371 (2003).
30. Intergovernmental Panel on Climate Change. *Climate Change 2001: The Scientific Basis.* http://www.grida.no/climate/ipcc_tar/wg1/figts-22.htm (2001).

Supplementary Information accompanies the paper on **www.nature.com/nature**.

Acknowledgements We thank the following for many contributions: E. Bolitho, V. Perez Canhos, D. A. L. Canhos, S. Carver, S. L. Chown, S. Fox, M. Kshatriya, D. Millar, A. G. Navarro-Sigüenza, R. S. Pereira, B. Reyers, E. Martínez-Meyer, V. Sánchez-Cordero, J. Soberón, D. R. B. Stockwell, W. Thuiller, D. A. Vieglais and K. J. Wessels, researchers involved in the Projeto de Cooperação Técnica Conservação e Manejo da Biodiversidade do Bioma Cerrado, EMBRAPA Cerrados, UnB, Ibama/DFID e RBGE/Reino Unido, and the European Bird Census Council. We thank G. Mace, J. Malcolm and C. Parmesan for valuable discussions, many funding agencies for support, and B. Orlando and others at IUCN for bringing together many of the coauthors at workshops. Comments from J. A. Pounds and S. Pimm greatly improved the manuscript.

Authors' contributions The fourth and subsequent authors are alphabetically arranged and contributed equally.

Competing interests statement The authors declare that they have no competing financial interests.

Correspondence and requests for materials should be addressed to C.D.T. (c.d.thomas@leeds.ac.uk).

Derivation of embryonic germ cells and male gametes from embryonic stem cells

Niels Geijsen[1,2], Melissa Horoschak[1,3], Kitai Kim[1,3], Joost Gribnau[1], Kevin Eggan[4] & George Q. Daley[1,3]

[1]*Whitehead Institute for Biomedical Research, 9 Cambridge Center, Cambridge, Massachusetts 02142, USA*
[2]*Center for Regenerative Medicine and Technology, Massachusetts General Hospital, Boston, Massachusetts 02114, USA*
[3]*Department of Biological Chemistry and Molecular Pharmacology, Harvard Medical School, and Division of Pediatric Hematology/Oncology, The Children's Hospital and Dana Farber Cancer Institute, Boston, Massachusetts 02115, USA*
[4]*Department of Molecular and Cellular Biology, Harvard University, 7 Divinity Avenue, Cambridge, Massachusetts 02138, USA*

Egg and sperm cells (gametes) of the mouse are derived from a founder population of primordial germ cells that are set aside early in embryogenesis. Primordial germ cells arise from the proximal epiblast, a region of the early mouse embryo that also contributes to the first blood lineages of the embryonic yolk sac[1]. Embryonic stem cells differentiate *in vitro* into cystic structures called embryoid bodies consisting of tissue lineages typical of the early mouse embryo[2,3]. Because embryoid bodies sustain blood development, we reasoned that they might also support primordial germ cell formation. Here we isolate primordial germ cells from embryoid bodies, and derive continuously growing lines of embryonic germ cells. Embryonic germ cells show erasure of the

methylation markers (imprints) of the *Igf2r* and *H19* genes, a property characteristic of the germ lineage. We show that embryoid bodies support maturation of the primordial germ cells into haploid male gametes, which when injected into oocytes restore the somatic diploid chromosome complement and develop into blastocysts. Our ability to derive germ cells from embryonic stem cells provides an accessible *in vitro* model system for studies of germline epigenetic modification and mammalian gametogenesis.

We differentiated embryonic stem (ES) cells according to our standard methods[4], and isolated messenger RNA from whole embryoid bodies (EBs) at several time points. We used polymerase chain reaction with reverse transcription (RT–PCR) to detect expression of genes implicated in ES cell pluripotency (the POU domain transcription factor *Oct4*) and germ cell development, including stella and fragilis (*Fgls*)[5], and a set of genes that are exclusively expressed in the germ line and are absent from somatic tissues (*Dazl*, *Piwil2*, *Rnf17*, *Rnh2*, *Tdrd1* and *Tex14*)[6–9]. All of these genes were expressed in undifferentiated ES cells, and a subset underwent rapid extinction with EB formation (Fig. 1). *Rnh2*, *Tdrd1* and *Tex14* decreased to undetectable levels very early in EB development (day 3–4), suggesting efficient differentiation and commitment to distinct cell fates. Stella and *Fgls* expression declined immediately on EB formation, but low levels persisted over the course of EB differentiation.

Expression of the surface antigen SSEA1, a marker of pluripotent ES cells, also wanes on EB development, but rare SSEA1 positive (SSEA1$^+$) cells persist in differentiated EBs[10]. We differentiated ES cells carrying an *Oct4*-promoter-driven green fluorescent protein (GFP) reporter gene[11], and observed a similar overall decrease in GFP$^+$ cell populations upon EB differentiation, as well as a persistent rare population of GFP$^+$ cells (data not shown). Although these might represent residual undifferentiated ES cells, SSEA1 and *Oct4* expression are also features of primordial germ cells (PGCs). We thus sought to determine whether these SSEA1$^+$/Oct4$^+$ cells within EBs represented residual undifferentiated ES cells or true PGCs.

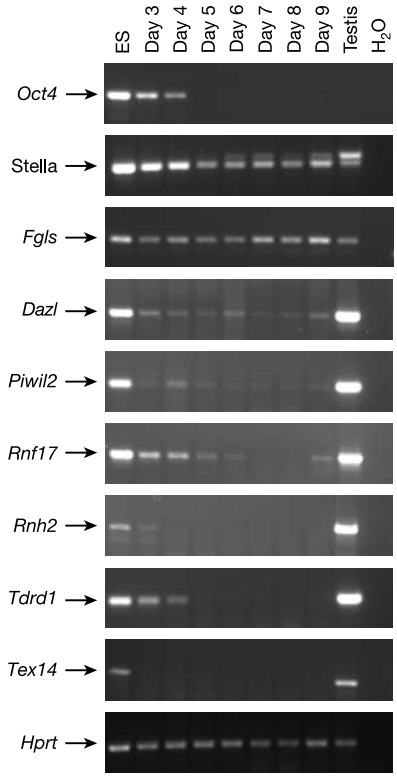

Figure 1 Expression of germ-cell-specific genes during EB development. RNA was prepared from ES cells, day 3–9 EBs and adult testis, and processed for RT–PCR. *Hprt* served as a control. Stella is expressed at high levels in primordial germ cells and oocytes but is almost absent from adult testis[5]. *Fgls* is expressed in the cells surrounding the germ cells[5]. *Dazl* is expressed only in germ cells in both testis and ovary[7,29]. *Piwil2*, *Rnf17*, *Rnh2*, *Tdrd1* and *Tex14* are germ-cell-specific and expressed in the male gonad[6].

There is a lack of markers that can suitably distinguish between ES cells and PGCs; however, retinoic acid acts to rapidly differentiate ES cells while stimulating proliferation of PGCs, and can therefore be used to distinguish between these two cell populations[12]. We plated ES cells or cells derived from EBs onto a mouse embryonic feeder (MEF) cell layer and cultured the cells for 7 days in the presence of 2 μM retinoic acid (Fig. 2a). We then quantified the residual SSEA1$^+$ cells. In retinoic acid-treated ES cells, greater than 99% of cells extinguished SSEA1 expression. In contrast, in retinoic acid-treated cultures of EB-derived cells, a significant percentage of SSEA1$^+$ cells persisted and expanded modestly in culture, with an apparent wave of formation peaking at around day 5 (Fig. 2b). Cells that differentiated for 5 days in retinoic acid were fixed and stained for alkaline phosphatase. Very few cells positive for alkaline phosphatase persisted in the retinoic acid-treated ES cell cultures (Fig. 2c, left panel). In contrast, large colonies of cells positive for alkaline phosphatase surrounded by motile cells that resembled migratory PGCs were abundant in retinoic acid-treated cultures of EB-derived cells (Fig. 2c, right panel). This differential effect of retinoic acid strongly suggested that the SSEA1$^+$ population of cells from EBs were PGCs.

To obtain conclusive evidence that the retinoic acid-resistant ES-like colonies were indeed PGCs, we analysed whether these cells manifested erasure of epigenetic imprints; this is a unique property of PGCs that is maintained in PGC-derived embryonic germ cells[13]. Imprinting of the *Igf2r* gene is determined by parental origin, with expression only from the maternal allele[14]. A specific region of the *Igf2r* gene has been identified, differentially methylated region 2 (DMR2), which is hypermethylated only on the maternally inherited allele[15]. We isolated SSEA1$^+$ cells from EBs at different time points and cultured the cells for 7 days in the presence of retinoic acid. Individual retinoic acid-resistant colonies were isolated and expanded on gelatinized tissue culture plastic in the presence of leukaemia inhibitory factor (LIF), stem cell factor (SCF) and basic fibroblast growth factor; these are conditions that support the derivation of embryonic germ cells[16,17]. We analysed the methylation status of DMR2 in independent clones of the parental ES cell line and in candidate embryonic germ clones by restriction digestion of the genomic DNA with *Pvu*II and the methylation-sensitive enzyme *Mlu*I. Independent ES cell clones demonstrated a somatic methylation profile in which only one allele was digested (Fig. 2d, top panel, lanes 1–5). Most of the day 4 EB-derived embryonic germ cell clones displayed a similar somatic imprinting profile (Fig. 2d, top panel, lanes 6–9), with the exception of one clone in which methylation was erased (Fig. 2d, top panel, lane 10), as demonstrated by digestion of both alleles. Notably, at day 7 of EB development, 6 of 7 embryonic germ-like cells showed an unmethylated pattern (Fig. 2d, top panel, lanes 11–16), and at day 10 of EB development all embryonic germ clones had lost imprinting of the *Igf2r* gene. Similar results were obtained showing erasure of the methylation marker at the *H19*/*Igf2* locus (Fig. 2d, bottom panel). These data demonstrate that the EB-derived PGCs display phenotypic and biological properties of PGCs developing *in vivo*.

We then used immunomagnetic bead sorting to isolate SSEA1$^+$ candidate PGCs from differentiated EBs, and used RT–PCR to analyse expression of germ-cell-specific markers. *Oct4* was

expressed in the SSEA1$^+$ population throughout EB development (Fig. 3a, left panel). *Oct4* expression was almost undetectable in the SSEA1-negative (SSEA1$^-$) fraction, demonstrating the effectiveness of the SSEA1 selection (Fig. 3a, right panel). *Tex14* and *Rnh2*, which demonstrated a rapid downregulation on EB differentiation in the whole EB population, became undetectable in the purified SSEA1$^+$ fraction of early EBs (days 3, 4; Fig. 3b). At day 5 expression levels of these genes rose, and by day 6 they reached a level comparable to ES cells. Although less marked than *Tex14* and *Rnh2*, expression of *Piwil2* and *Dazl* follows a similar pattern of increased expression over time in SSEA1$^+$ differentiated EB-derived cell populations. This suggests that the developing EB supports a cellular environment similar to the early embryonic microenvironment in which PGCs are found.

To determine whether the PGCs arise in a defined region of the EB, we used immunohistochemistry to simultaneously visualize CD41$^+$ haematopoietic cells[18] and SSEA1$^+$ germ cells in cryosections of 7-day-old EBs (Fig. 3c). Similar to the developing embryo, the SSEA1$^+$ PGCs in the developing EB exist in close juxtaposition to the cells of the developing haematopoietic system. The co-localization of nascent blood and germ cell populations in the peripheral zones of the developing EB raises interesting questions about their clonal origins and the microenvironment that specifies their distinct cell fates.

We next investigated whether the EB-derived PGCs undergo further differentiation into functional gametes. We analysed the expression of *Sry*, a male gene that determines germ cell fate. *Sry* expression was first detected in day 5 EBs, heralding initiation of a male germ cell developmental programme (Fig. 4a). Germ cell nuclear factor (*Gcnf*) has a role in confining *Oct4* expression to the germ line[19]. We observed transient expression of *Gcnf* starting at day 7 and peaking at around day 11, suggesting a temporal window during which the germ cells become fully specified. At about day 11 of EB differentiation we found a strong upregulation of acrosin and haprin, genes tightly associated with male germ cell development (Fig. 4b). Acrosin is part of the acrosomal complex transcribed as proacrosin in the diploid germ cell population[20], whereas haprin is a member of the RING finger–B box–coiled-coil family of transcription factors, which have a role in spermatogenesis and the formation of germ cell tumours[21–23]. Our observation of upregulation of genes associated with male germ cell maturation prompted us to investigate the presence of stromal supporter cells. Indeed, we detected the message for the luteinizing hormone/gonadotropin receptor (LH-R) as well as müllerian inhibiting substance (MIS); these are markers of Leydig and Sertoli cells, respectively. We failed to detect expression of zona pellucida proteins Zp1 and Zp2, whereas Zp3 is expressed in ES cells and early EBs (Fig. 4b), suggesting that within the context of EB differentiation, the default programme of female gametogenesis is suppressed. Indeed when comparing the expression of two genes specific for male germ cell differentiation, *AZ1* and ret finger protein (*Rfp*), we observed exclusive expression of these genes in EBs derived from male (XY) but not female (XX) ES cells (Fig. 4c).

To investigate whether male germ cells undergo meiosis in the

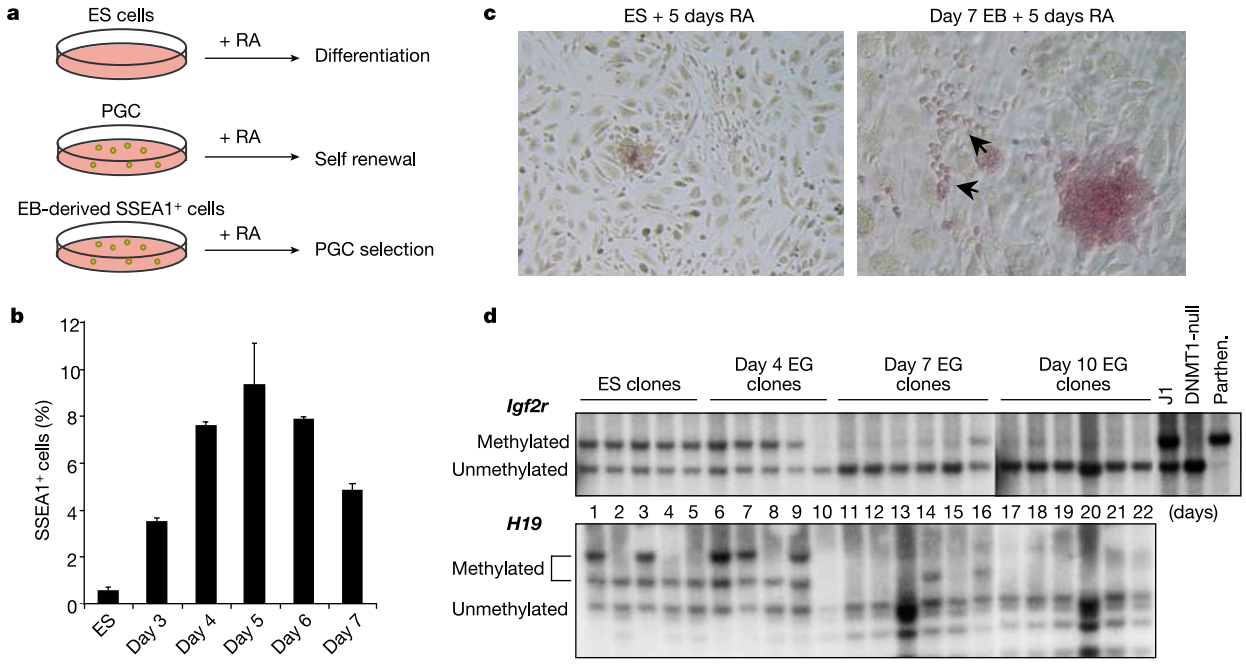

Figure 2 Development of primordial germ cells in the differentiating EB. **a**, Effects of treatment with retinoic acid (RA) on EB-derived cells. Retinoic acid differentiates ES cells (top panel) but supports PGCs[12] (middle panel). Culture of EB-derived SSEA1$^+$ cells in the presence of retinoic acid selects for PGCs that retain germ cell marker expression (bottom panel). **b**, SSEA1$^+$ cells were isolated from EBs of different ages by immunomagnetic beads, cultured in retinoic acid for 7 days, and SSEA1 expression was analysed by flow cytometry. The percentage of GFP$^+$ ES and EB-derived cells expressing SSEA1 is plotted ($n = 3$) **c**, Alkaline phosphatase (AP) expression on ES cells (left panel) and day 7 EB-derived cells (right panel) after 5 days of culture in retinoic acid. The day 7 EB-derived cells formed large colonies of cells positive for alkaline phosphatase that resembled PGCs on gross inspection[17]. Cells positive for alkaline phosphatase migrated out of the large colony (arrowheads). **d**, Imprint erasure of *Igf2r* and *H19*/*Igf2* loci. Top panel, DMR2 region of *Igf2r* locus. Southern analysis of genomic DNA from individual ES and EB-derived embryonic germ clones digested with *Pvu*II and *Mlu*I is shown. Bottom panel, *H19*/*Igf2* locus. The same clones as in the top panel were digested with *Sac*I and *Hha*I. The day of EB development at which individual embryonic germ clones were derived is indicated. Control lanes include J1 ES cells (somatic methylation profile), methylation-deficient DNMT1^{null} ES cells[30] and parthenogenetic (parthen.) ES cells (showing a maternal methylation pattern on both *Igfr2* alleles).

context of the EB, we immunostained cell populations with an antibody that specifically recognizes male meiotic germ cells (FE-J1[24]), and analysed these cells for DNA content using the fluorescent DNA-binding dye Hoechst 33342. In the testes of adult mice, both FE-J1$^+$ and haploid (1C) cells are readily identified (Fig. 4d, left column of top and middle panels). Analysing the FE-J1$^+$ cell population for DNA content shows that this marker of male germ cells recognizes a minor diploid (2C) population of primary spermatocytes and a predominant population of cells with a haploid (1C) DNA complement, as reported[24] (Fig. 4d, bottom panel, left). In the EB cell suspension, haploid (1C) cells are discernable but obscured by a range of apoptotic cells with sub-2C DNA content (Fig. 4d, middle panel, right). However, when only the cells positive for the FE-J1 antibody are analysed, a distinct haploid (1C) population is observed, representing the predominant class of FE-J1-staining cells (Fig. 4d, bottom panel, right). The low proportion of antibody-positive cells (0.01%) and the relatively high ratio between diploid (2C) primary spermatocytes and haploid (1C) cells suggests that meiosis is highly inefficient in EBs. This experiment, however, demonstrates that the EB microenvironment is permissive for male germ cell development and meiotic maturation.

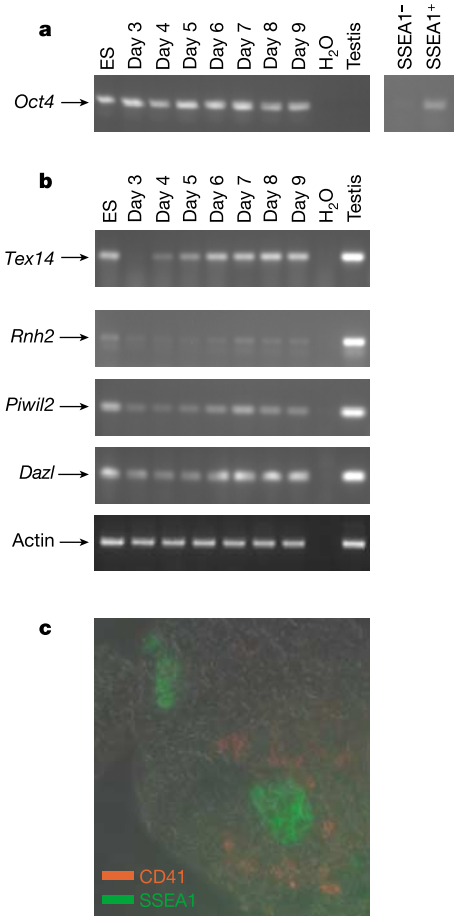

Figure 3 RT–PCR detection of germ-cell-specific genes in SSEA1$^+$ cells isolated from developing EBs. **a**, Expression of *Oct4* during EB development (left panel) and in SSEA1$^+$ and SSEA1$^-$ fractions derived by immunomagnetic sorting. Flow cytometric analysis demonstrates >90% purity in the SSEA1$^+$ fraction and >99% purity of the SSEA1$^-$ fraction (data not shown). **b**, Expression of *Tex14*, *Rnh2*, *Piwil2* and *Dazl* assayed by RT–PCR. Actin served as a control. **c**, Immunohistochemistry of germ cell and haematopoietic development in day 7 EBs. EBs were cryosectioned and stained with CD41–fluorescein isothiocyanate (green) to mark early haematopoietic cells and SSEA1–PE (red) to visualize germ cell development.

We further analysed the FE-J1$^+$ cells by immunofluorescence microscopy. The FE-J1 antibody recognizes the anterior acrosome on early and late pachytene spermatocytes and on round spermatids[24]. As can be seen in Fig. 4e, FE-J1$^+$ cells isolated from testes (top panel) or from day 20 EBs (bottom panel) demonstrate polarized apical perinuclear staining, indicating that the EB-derived cells have a similar morphology to testis-derived haploid cells, and possibly represent round spermatids.

Finally, we investigated the biological function of the EB-derived haploid cells and assayed their capacity to fertilize oocytes. We isolated FE-J1$^+$/GFP$^+$ haploid cells from day 20 EBs by flow cytometry, and performed intracytoplasmic injection into recipient oocytes. Five separate microinjection experiments performed in two independent laboratories produced comparable results. Approximately 50% of the injected oocytes supported cleavage to the 2-cell stage ($n = 125$), with 20% displaying progression to blastocysts. Figure 4f shows four representative blastocysts expressing the GFP transgene, indicating successful complementation of the oocyte genome by the EB-derived haploid cells. Furthermore, fluorescence *in situ* hybridization (FISH) using probes directed against an autosomal locus and markers on the X and Y chromosome demonstrate a normal diploid chromosome complement and expected ratios of male (XY) and female (XX) embryos (Fig. 4g). Efforts are underway to determine whether embryos arising from fertilization with EB-derived male gametes will develop normally after uterine transfer.

Germ cell development remains a largely unexplored but fascinating process of cell fate specification. Germ cells represent a privileged class of cells, given responsibility for perpetuating pluripotency and ensuring propagation of the gene pool. The genetic mechanisms that account for maintenance of pluripotency and restrict somatic differentiation are beginning to yield to molecular analyses[5], but an *in vitro* model system that recapitulates germ cell specification will greatly facilitate these studies.

Recently, Schöler and colleagues reported the generation of oocytes from mouse ES cells in culture[25]. The reported differentiation happened spontaneously over a period of nearly 50 days. In contrast to our method of ES cell differentiation into EBs, Schöler and colleagues used bulk two-dimensional differentiation on tissue culture plastic, in which both male and female lines of ES cells yielded oocytes. Given our observation of male germ cell development, we speculate that EBs may preserve more of the tissue organization reflective of the embryonic gonadal ridge, thereby enabling male germ lineage specification. In support of this notion, we detected expression of the müllerian inhibiting substance in EBs by RT–PCR. While this manuscript was under review, Noce and colleagues reported the successful derivation of male lineage germ cells from ES cells *in vitro*[26]. Our work corroborates and extends this report by demonstrating the erasure of methylation markers at imprinted loci and the successful fertilization of oocytes by the ES-derived male gametes.

Although EBs may not reflect the precise temporal and spatial features of embryonic development, their ready derivation from ES cells *in vitro* has proven valuable for genetic studies of tissue differentiation, by linking gene deletions or ectopic transgene expression to specific cellular phenotypes. We have demonstrated the *in vitro* differentiation of ES cells into primordial germ cells, which proliferate in response to retinoic acid and give rise to embryonic germ-cell-like clones that undergo erasure of imprints. We are currently using this *in vitro* system to investigate whether EB differentiation sustains a male germ cell niche that enables the proper restoration of male imprints, thereby affording an *in vitro* system to address the genetic and biochemical mechanisms of this fundamental epigenetic modification. As demonstrated by molecu-

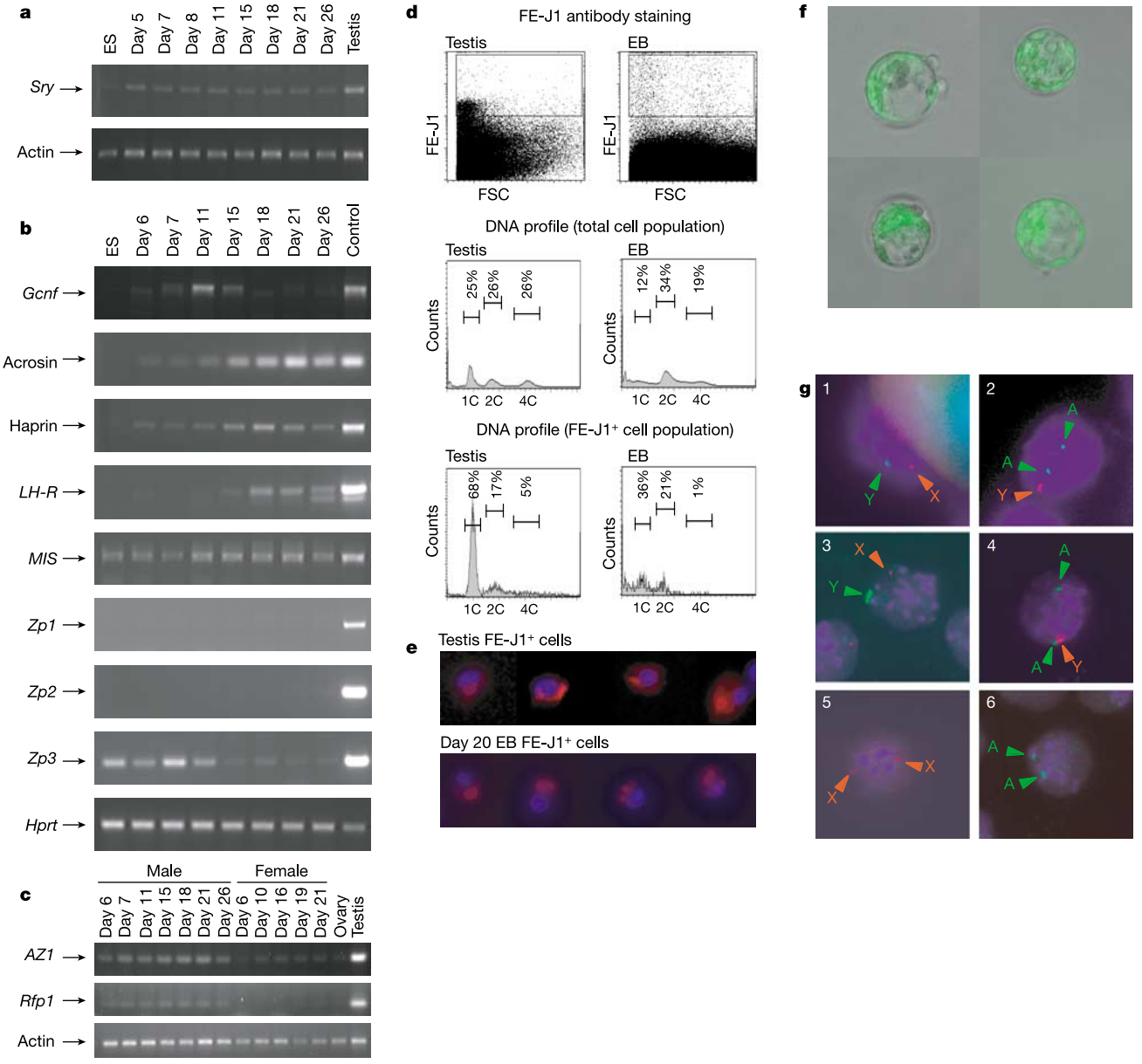

Figure 4 EBs support differentiation of haploid male germ cells that support fertilization of oocytes. **a**, Expression of *Sry* in developing EBs analysed by RT–PCR (top panel). **b**, Expression of genes regulating male germ cell specification during EB development. *Gcnf* helps restrict *Oct4* expression to the germ line[19]. Acrosin, acrosomal protein with a role in oocyte interaction[20]; haprin, haploid germ-cell-specific RING finger protein; *LH-R* and *MIS*, markers for Leydig and Sertoli cells, respectively; Zp1–3, proteins of the oocyte zona pellucida. *Hprt* served as a control. **c**, Expression of male germ-cell-specific genes in male or female EBs assayed by RT–PCR. Control RNA from ovary or testis is shown. **d**, Identification of haploid male germ cells in adult testis (left) or day 13 EBs (right) by immunostaining with the FE-J1 antibody[24]. Cells were stained with the DNA-binding dye Hoechst 33342 to reveal DNA content. 1C, haploid; 2C, G0/G1 phase; 4C, G2/M phase. **e**, Immunohistochemistry of the FE-J1$^+$ cells sorted in **d**. FE-J1–PE, red; nuclear Hoechst 33342, blue. **f**, Fluorescence image of blastocysts derived from intracytoplasmic injection of oocytes with EB-derived FE-J1$^+$ haploid cells. **g**, FISH analysis of control ES cells and morula stage embryos, with fluorescence signals indicated by arrows. Panels 1 (X and Y chromosome markers) and 2 (autosomal (κ light chain) and Y chromosome markers) show embryos derived from intracytoplasmic oocyte injection of FE-J1$^+$ haploid cells. Panels 3 (X and Y chromosome markers) and 4 (autosomal (κ light chain) and Y chromosome markers) show control male ES cells. Panels 5 (X and Y chromosome markers; note two X and absence of Y signals) and 6 (autosomal (κ light chain) and Y chromosome markers; note absence of Y signal) show control female ES cells.

lar analysis, the EBs support a programme of male germ cell differentiation, culminating in the formation of haploid cells that manifest the morphology and fertilization potential of male haploid germ cells of the round spermatid stage. Our report, together with the recent demonstration of oocyte and sperm generation from ES cells[25,26], signals a new realm of possibilities for investigating germ cell development, epigenetic reprogramming and germline gene modification. □

Methods

Mouse strains and ES cells

C57BL/6-TGN(ACTbEGFP) mice were from Jackson Laboratories[27]. 129SvEv mice were from Taconic. ES cells were derived from an F_1 cross between C57BL/6-TGN(ACTbEGFP)1Osb and 129SvEv.

Cell culture

ES cells were maintained on irradiated MEFs in DME/15% IFS, 0.1 mM non-essential amino acids (GIBCO), 2 mM glutamine, penicillin/streptomycin (GIBCO), 0.1 mM

β-mercaptoethanol, and 1,000 U ml^{-1} LIF (Invitrogen). For EB differentiation, ES cells were digested with trypsin, collected in EB medium (IMDM/15% IFS, 200 μg ml^{-1} iron-saturated transferrin (Sigma), 4.5 mM monothiolglycerol (Sigma), 50 μg ml^{-1} ascorbic acid (Sigma) and 2 mM glutamine) and plated for 45 min to allow MEFs to adhere. Non-adherent cells were collected and plated in hanging drops at 200 cells per 30 μl droplet in an inverted bacterial Petri dish. EBs were collected from the hanging drops at day 3 and transferred into 10 ml EB medium in slowly rotating 10 cm Petri dishes. At day 4, EBs were fed by exchanging half of their spent medium. Cells were collected by collagenase treatment and re-suspension in cell dissociation buffer (Invitrogen).

RT–PCR

RT–PCR amplifications were titrated to be within a linear range of amplification. Primers used are: *Oct4*(f) 5′-GTGGATTCTCGAACCTGGCT-3′, *Oct4*(r) 5′-GTCTCCAGACTCCACCTCAC-3′; stella(f) 5′-CAGCCGTACCTGTGGAGAACAAGAG-3′, stella(r) 5′-AGCCCTGGGCCTCACAGCTT-3′; *Fgls*(f) 5′-TTGCTCCGCACCATGAACCA-3′, *Fgls*(r) 5′-TGAAGCACTTCAGGACCGGA-3′; *Dazl*(f) 5′-GCCAGCACTCAGTCTTCATC-3′, *Dazl*(r) 5′-GTTGGAGGCTGCATGTAAGT-3′; *Piwil2*(f) 5′-CCGTCATGAAGGAGAGCTCG-3′, *Piwil2*(r) 5′-GGAACGACTCTGTGCTGGAT-3′; *Rnf17*(f) 5′-GACACACAGTCTAACAGAGG-3′, *Rnf17*(r) 5′-AGGACAGCAGCATCTACCTT-3′; *Rnh2*(f) 5′-CATAAGTGGCAACGAAGAGC-3′, *Rnh2*(r) 5′-GTTACAGGCTGCTACCATCA-3′; *Tdrd1*(f) 5′-GCAGTTCTGCTCTGTCAAGG-3′, *Tdrd1*(r) 5′-CAGAGCGTGGAATCACATGG-3′; *Tex14*(f) 5′-GAAGCTTGAGCAGGAGGTAG-3′, *Tex14*(r) 5′-TTCAGAAGACACAGACGCCA-3′; *Gcnf*(f) 5′-GTGGAAGACCAGGACGACGA-3′, *Gcnf*(r) 5′-CCTACTGGATGATAGTGTGG-3′; acrosin(f) 5′-CGGAGTCTACACAGCCACCT-3′, acrosin(r) 5′-GCATGAGTGATGAGGAGGTT-3′; haprin(f) 5′-CCAGAACATGAGACAGAGAG-3′, haprin(r) 5′-AGCAACTTCCTGAGCATACC-3′; *Hprt*(f) 5′-GCTGGTGAAAAGGACCTCT-3′, *Hprt*(r) 5′-CACAGGACTAGAACACCTGC-3′; *Sry*(f) 5′-TTACAGCCTGCAGTTGCCTC-3′, *Sry*(r) 5′-GGTCATAGAACTGCTGTTGC-3′; *MIS*(f) 5′-TTGGTGCTAACCCGTGGACTT-3′, *MIS*(r) 5′-GCAGAGCACGAACCAAGCGA-3′; *LH-R*(f) 5′-TGCAACCTCCTCAATCTGTC-3′, *LH-R*(r) 5′-AGCGTGGCAACCAGTAGGCT-3′; *Zp1*(f) 5′-GAGTGACTGTGTTGCCATAG-3′, *Zp1*(r) 5′-GCCACACTGGTCTCACTACG-3′; *Zp2*(f) 5′-GCTACACACATGACTCTCAC-3′, *Zp2*(r) 5′-GGTGACTCACAGTGGCACTC-3′; *Zp3*(f) 5′-TTGAGCAGAAGCAGTCCAGC-3′, *Zp3*(r) 5′-CGGTTGCCTTGTGGATGGTC-3′; actin(f) 5′-ACCAACTGGGACGATATGGAGAAGA-3′, actin(r) 5′-CTCTTTGATGTCACGCACGATTTC-3′.

Immunomagnetic isolation of SSEA1$^+$ cells

Cells collected from EBs were incubated (30 min) with a monoclonal antibody against SSEA1 (Hybridoma bank) at 4 °C in PBS/0.5% BSA. Cells were washed twice with ice-cold PBS/0.5% BSA before addition of immunomagnetic rat anti-mouse IgM beads (Dynal), and were incubated for 1 h at 4 °C with slow rotation. Magnetic separation of SSEA1$^+$ beads associated with the cells was performed according to the manufacturer's protocol.

Southern analysis

Genomic DNA was prepared from individual clones of the parental ES cell line or EB-derived embryonic germ cells. For the embryonic germ cell clones, SSEA1$^+$ cells were isolated at different days of EB development and cells were grown in the presence of retinoic acid for 7 days followed by 2 days of culture without retinoic acid. Individual clones were isolated and expanded on gelatinized tissue culture plastic in the presence of LIF to remove feeder cells. Genomic DNA was isolated and digested with *Pvu*II and *Mlu*I for the detection of *Igf2r* methylation, or with *Sac*I and *Hha*I for the analysis of *H19* imprints. DNA was separated on a 0.7% agarose gel and Southern blots were generated by standard methods. Filters were hybridized with a probe covering region 2 of the *Igf2r* receptor (pPP4).

FACS analysis

Testicular and EB-derived cell suspensions were obtained by enzymatic digest of the tissue. Briefly, cells were incubated at 37 °C for 15 min with digest buffer (0.1% collagenase IV, 0.2% hyaluronidase and 50 U ml^{-1} DNase (all Sigma)). Cells were then dissociated using cell dissociation buffer (Invitrogen), collected by centrifugation and a second digest was performed. Cell clumps were removed using a 70 μM strainer and cells were re-suspended in ice-cold RPMI plus 0.5% FBS. Cells were incubated with FE-J1, a haploid male germ-cell-specific antibody (Hybridoma bank[24]), for 30 min at 4 °C. The cells were washed twice with RPMI/0.5% FBS and incubated with phycoerythrin (PE)-conjugated rat anti-mouse IgM for 30 min at 4 °C. Cells were washed twice with RPMI/0.5% FBS, re-suspended in RPMI/0.5% FBS containing 2.5 μg ml^{-1} cytochalasin B (Sigma) and sorted on a Becton-Dickinson FACSCalibur.

Oocyte injections

Eight–ten-week-old B6D2F1/J mice (Jackson Laboratories) were used as oocyte donors. EB-derived donor cells were re-suspended in KSOM (Speciality Medium) containing 10% (w/v) polyvinyl alcohol (Sigma) and 0.01% (w/v) bovine serum albumin (Sigma). Intracytoplasmic injection into cumulus-free oocytes was carried out in H-KSOM containing 5 μg ml^{-1} cytochalasin B (Sigma) and 3% (w/v) sucrose at room temperature using a Nikon Eclipse TE300 microscope equipped with Narashige hydraulic micromanipulators and Hoffman modulation contrast. The injected oocytes were washed five times in KSOM to remove the cytochalasin. Reconstructed embryos were activated either in KSOM containing 10 μM calcium ionophore A23187 (Sigma) for 5 min, followed by 2 mM 6-dimethylaminopurine (Sigma) in KSOM at 37 °C in 5% CO_2 for 3 h, or for 5 h in Ca^{2+}-free medium containing 10 mM $SrCl_2$. Embryos were then washed five times in KSOM. Embryos were cultured in KSOM at 37 °C in 5% CO_2.

DNA-FISH

DNA-FISH was performed as described[28] with minor modifications. The zona was removed from embryos using acid tyrodase, and the morulae were incubated in a small drop of 0.075 M KCl on a slide for 5 min. Embryos were fixed by replacing the KCl with 3:1 methanol:acetic acid. Cells were permeabilized in 0.5% triton/PBS for 10 min, washed twice in PBS and dehydrated in 70%, 90% and 100% ethanol. Bacterial artificial chromosome (BAC) clones used for FISH analysis were from BACPAC resources and from Invitrogen. Autosomal sequences were detected with BAC RP23-20P21, which is specific for the κ light chain locus of immunoglobulin. X chromosomal sequences were detected with BAC CT7-228O4, which is specific for the *Irak1* locus. Y chromosomal sequences were detected with BAC RP24-507D23, which is specific for Y chromosomal repeats.

Received 26 June; accepted 24 November 2003; doi:10.1038/nature02247.
Published online 10 December 2003.

1. Lawson, K. A. & Hage, W. J. Clonal analysis of the origin of primordial germ cells in the mouse. *Ciba Found. Symp.* **182,** 68–84, 84–91 (1994).
2. Doetschman, T. C., Eistetter, H., Katz, M., Schmidt, W. & Kemler, R. The *in vitro* development of blastocyst-derived embryonic stem cell lines: formation of visceral yolk sac, blood islands and myocardium. *J. Embryol. Exp. Morphol.* **87,** 27–45 (1985).
3. Leahy, A., Xiong, J. W., Kuhnert, F. & Stuhlmann, H. Use of developmental marker genes to define temporal and spatial patterns of differentiation during embryoid body formation. *J. Exp. Zool.* **284,** 67–81 (1999).
4. Kyba, M., Perlingeiro, R. C. & Daley, G. Q. HoxB4 confers definitive lymphoid-myeloid engraftment potential on embryonic stem cell and yolk sac hematopoietic progenitors. *Cell* **109,** 29–37 (2002).
5. Saitou, M., Barton, S. C. & Surani, M. A. A molecular programme for the specification of germ cell fate in mice. *Nature* **418,** 293–300 (2002).
6. Wang, P. J., McCarrey, J. R., Yang, F. & Page, D. C. An abundance of X-linked genes expressed in spermatogonia. *Nature Genet.* **27,** 422–426 (2001).
7. Cooke, H. J., Lee, M., Kerr, S. & Ruggiu, M. A murine homologue of the human DAZ gene is autosomal and expressed only in male and female gonads. *Hum. Mol. Genet.* **5,** 513–516 (1996).
8. Seboun, E. *et al.* Gene sequence, localization, and evolutionary conservation of DAZLA, a candidate male sterility gene. *Genomics* **41,** 227–235 (1997).
9. Moore, F. L. *et al.* Human Pumilio-2 is expressed in embryonic stem cells and germ cells and interacts with DAZ (Deleted in AZoospermia) and DAZ-like proteins. *Proc. Natl Acad. Sci. USA* **100,** 538–543 (2003).
10. Zandstra, P. W., Le, H. V., Daley, G. Q., Griffith, L. G. & Lauffenburger, D. A. Leukemia inhibitory factor (LIF) concentration modulates embryonic stem cell self-renewal and differentiation independently of proliferation. *Biotechnol. Bioeng.* **69,** 607–617 (2000).
11. Bortvin, A. *et al.* Incomplete reactivation of Oct4-related genes in mouse embryos cloned from somatic nuclei. *Development* **130,** 1673–1680 (2003).
12. Koshimizu, U., Watanabe, M. & Nakatsuji, N. Retinoic acid is a potent growth activator of mouse primordial germ cells *in vitro*. *Dev. Biol.* **168,** 683–685 (1995).
13. Labosky, P. A., Barlow, D. P. & Hogan, B. L. Mouse embryonic germ (EG) cell lines: transmission through the germline and differences in the methylation imprint of insulin-like growth factor 2 receptor (Igf2r) gene compared with embryonic stem (ES) cell lines. *Development* **120,** 3197–3204 (1994).
14. Barlow, D. P., Stoger, R., Herrmann, B. G., Saito, K. & Schweifer, N. The mouse insulin-like growth factor type-2 receptor is imprinted and closely linked to the Tme locus. *Nature* **349,** 84–87 (1991).
15. Stoger, R. *et al.* Maternal-specific methylation of the imprinted mouse Igf2r locus identifies the expressed locus as carrying the imprinting signal. *Cell* **73,** 61–71 (1993).
16. Matsui, Y., Zsebo, K. & Hogan, B. L. Derivation of pluripotential embryonic stem cells from murine primordial germ cells in culture. *Cell* **70,** 841–847 (1992).
17. Resnick, J. L., Bixler, L. S., Cheng, L. & Donovan, P. J. Long-term proliferation of mouse primordial germ cells in culture. *Nature* **359,** 550–551 (1992).
18. Mikkola, H. K., Fujiwara, Y., Schlaeger, T. M., Traver, D. & Orkin, S. H. Expression of CD41 marks the initiation of definitive hematopoiesis in the mouse embryo. *Blood* **101,** 508–516 (2003).
19. Fuhrmann, G. *et al.* Mouse germline restriction of Oct4 expression by germ cell nuclear factor. *Dev. Cell* **1,** 377–387 (2001).
20. Wassarman, P. M. Mouse gamete adhesion molecules. *Biol. Reprod.* **46,** 186–191 (1992).
21. Cao, T., Shannon, M., Handel, M. A. & Etkin, L. D. Mouse ret finger protein (rfp) proto-oncogene is expressed at specific stages of mouse spermatogenesis. *Dev. Genet.* **19,** 309–320 (1996).
22. Ogawa, S. *et al.* Molecular cloning of a novel RING finger-B box-coiled coil (RBCC) protein, terf, expressed in the testis. *Biochem. Biophys. Res. Commun.* **251,** 515–519 (1998).
23. Tezel, G., Nagasaka, T., Shimono, Y. & Takahashi, M. Differential expression of RET finger protein in testicular germ cell tumors. *Pathol. Int.* **52,** 623–627 (2002).
24. Fenderson, B. A., O'Brien, D. A., Millette, C. F. & Eddy, E. M. Stage-specific expression of three cell surface carbohydrate antigens during murine spermatogenesis detected with monoclonal antibodies. *Dev. Biol.* **103,** 117–128 (1984).
25. Hubner, K. *et al.* Derivation of oocytes from mouse embryonic stem cells. *Science* **300,** 1251–1256 (2003).
26. Toyooka, Y., Tsunekawa, N., Akasu, R. & Noce, T. Embryonic stem cells can form germ cells *in vitro*. *Proc. Natl Acad. Sci. USA* **100,** 11457–11462 (2003).
27. Okabe, M., Ikawa, M., Kominami, K., Nakanishi, T. & Nishimune, Y. 'Green mice' as a source of ubiquitous green cells. *FEBS Lett.* **407,** 313–319 (1997).
28. Selig, S., Okumura, K., Ward, D. C. & Cedar, H. Delineation of DNA replication time zones by fluorescence *in situ* hybridization. *EMBO J.* **11,** 1217–1225 (1992).
29. Reijo, R. *et al.* Mouse autosomal homolog of DAZ, a candidate male sterility gene in humans, is expressed in male germ cells before and after puberty. *Genomics* **35,** 346–352 (1996).
30. Li, E., Bestor, T. H. & Jaenisch, R. Targeted mutation of the DNA methyltransferase gene results in embryonic lethality. *Cell* **69,** 915–926 (1992).

Acknowledgements The authors thank S. L. Opitz, N. Watson and E. Dikovskaia for technical support; K. Hochedlinger and T. Holm for assistance with intracytoplasmic oocyte injection; and W. Lensch for critical revisions of the manuscript. This work was supported by grants from the National Institutes of Health, the National Science Foundation Biotechnology Process Engineering Center, and the Dutch Cancer Society 'Koningin Wilhelmina fonds'. G.Q.D. is a Birnbaum Scholar of the Leukemia and Lymphoma Society of America. J.G. was sponsored by the Human Frontiers Science Foundation. K.E. is a Junior Fellow in the Harvard Society of Fellows.

Competing interests statement The authors declare that they have no competing financial interests.

Correspondence and requests for materials should be addressed to G.Q.D. (george.daley@childrens.harvard.edu).

T-cell priming by dendritic cells in lymph nodes occurs in three distinct phases

Thorsten R. Mempel, Sarah E. Henrickson & Ulrich H. von Andrian

The CBR Institute for Biomedical Research, Department of Pathology, Harvard Medical School, 200 Longwood Avenue, Boston, Massachusetts 02115, USA

Primary T-cell responses in lymph nodes (LNs) require contact-dependent information exchange between T cells and dendritic cells (DCs). Because lymphocytes continually enter and leave normal LNs, the resident lymphocyte pool is composed of non-synchronized cells with different dwell times that display heterogeneous behaviour in mouse LNs *in vitro*[1–3]. Here we employ two-photon microscopy *in vivo* to study antigen-presenting DCs and naive T cells whose dwell time in LNs was synchronized. During the first 8 h after entering from the blood, T cells underwent multiple short encounters with DCs, progressively decreased their motility, and upregulated activation markers. During the subsequent 12 h T cells formed long-lasting stable conjugates with DCs and began to secrete interleukin-2 and interferon-γ. On the second day, coinciding with the onset of proliferation, T cells resumed their rapid migration and short DC contacts. Thus, T-cell priming by DCs occurs in three successive stages: transient serial encounters during the first activation phase are followed by a second phase of stable contacts culminating in cytokine production, which makes a transition into a third phase of high motility and rapid proliferation.

Naive T cells recirculate continually between the blood and LNs to search for antigen[4]. The intranodal encounter of a peptide–major histocompatibility complex (MHC) complex that is recognized by a T-cell antigen receptor (TCR) will only result in full-fledged T cell activation upon co-stimulation provided by mature DCs. These professional antigen-presenting cells collect antigens in peripheral tissues and migrate to LNs through lymph vessels. T-cell priming by DCs induces activation markers, cytokine secretion, and proliferation. Several reports have analysed the dynamics of T-cell–DC interactions in excised LNs, but the methods and results have been variable and it is unknown how the absence of lymph and blood flow or innervation influences T-cell–DC interactions[1–3,5]. There is therefore still no comprehensive description of what happens in a truly physiological setting when naive T cells enter LNs that contain antigen-presenting DCs.

We have used two-photon microscopy[6] to study lymphocyte migration and interactions with DCs within popliteal LNs of anaesthetized mice. Our preparation preserved physiological blood and lymph flow[7], whereas, in our hands, lymph flow was compromised when we attempted to adapt the well-established inguinal lymph-node preparation to two-photon imaging[8,9] (not shown). Recipient mice received footpad injections of fluorescent DCs, which entered lymph vessels and accumulated in the popliteal LN during the following day. Differentially tagged TCR transgenic $CD8^+$T cells were injected intravenously 18 h later (Fig. 1a). T cells homed rapidly through high endothelial venules (HEVs) into popliteal LNs[7], where they constituted 1–2% of all $CD8^+$ cells 2 h after injection. At this point, further lymphocyte homing was blocked by the injection of anti-L-selectin[10]. This ensured that all imaged T cells had entered popliteal LNs during the initial 2-h window and enabled us to study synchronized resident cells during the subsequent 2 days.

Initially, we examined the phenotype of injected DCs that migrated to draining LNs (Fig. 1b). Immature splenic $CD11c^+$ DCs from $CD45.1^+$ donors were injected into $CD45.2^+$ congenic recipients. Because immature DCs express little or no CCR7—a chemokine receptor required for DC migration into lymphatics and within LNs[11]—we co-injected lipopolysaccharide (LPS; 10 ng), which induces DC maturation and CCR7 expression[12]. Consequently, DCs recovered from popliteal LNs were mature and either $CD11b^+CD8\alpha^-$ or $CD11b^-CD8\alpha^{low/-}$. $CD8\alpha^{high}$ input DCs were rarely detected in LNs. This might reflect an inability of $CD8\alpha^{high}$ DCs to migrate to LNs, or the downregulation of CD8α during transit.

To examine DCs *in situ*, we administered footpad injections of red fluorescent DCs and analysed their behaviour within popliteal LNs. After 20 h a fraction of migrated DCs (about 20–50%) resided in the subcapsular sinus and the superficial cortex. The remainder congregated in distinct regions within the deep cortex, where they localized with homed T cells (Supplementary Fig. S1a). A reason for the non-uniform distribution of DCs in the T cell area became apparent after fluorescein isothiocyanate–dextran injection to delineate blood vessels. In line with recent observations[13], many DCs lined up around HEVs in strategic positions to interact with newly homed T cells (Supplementary Fig. S1b; Supplementary Information 2, 3). This distribution pattern became less apparent at day 2 or 3 after injection (Supplementary Information 4).

One day after injection, DCs in T-cell areas were remarkably motile, whether they presented antigen to T cells or not (Fig. 1c–g; Supplementary Information 5). The median three-dimensional (3D) instantaneous velocity was 6.6 μm min^{-1} (Fig. 1e), which is in good agreement with measurements of two-dimensional velocities in explanted LNs[3]. Individual DCs followed random paths without apparent directional bias. Even sessile DCs constantly extended and retracted dendrites and pseudopods. The motility of both antigen-pulsed and control DCs was highest between 2 and 8 h after T-cell transfer (20–26 h after DC injection) and decreased over time (Fig. 1f, g; Supplementary Information 5). This progressive decrease in motility might reflect DC 'exhaustion', which has been proposed to occur after LPS activation[14].

Migratory dynamics in LNs were closely dependent on physiological conditions: T cells and DCs stopped migrating and assumed a round shape within minutes after cardiovascular arrest (Supplementary Information 6), even with a tissue temperature maintained at 36 °C, a requirement for interstitial T-cell migration[2]. In living animals without DC injection, intranodal T cells moved rapidly, reaching peak 3D velocities of 40 μm min^{-1} (Fig. 2a–c; Supplementary Information 7). In LNs draining DC-injected footpads, 3D velocities were equivalent (Fig. 2c, d) but T cells turned at steeper angles and covered a smaller volume of the paracortex, resulting in decreased motility coefficients, even when DCs carried no antigen (Fig. 2e, f). Mean T-cell displacement plots in the antigen-containing LNs revealed a plateau at about 15 μm displacement (Fig. 2e), indicating confined motility[15]. Thus, DC plus LPS injections induced LN paracortex partitioning into smaller compartments in which incoming T cells were retained, perhaps owing